

# Carbon Nanotube Sponges

By Xuchun Gui, Jinqun Wei, Kunlin Wang, Anyuan Cao,\* Hongwei Zhu, Yi Jia, Qinke Shu, and Dehai Wu\*

Carbon nanotubes (CNTs) are nanoscale structures with excellent mechanical and electronic properties. Production of macroscopic, engineered structures based on assembled CNTs with controlled orientation and configuration is an important step towards practical applications. To this end, CNT-based macrostructures have been fabricated in various forms such as vertically aligned arrays via direct growth,<sup>[1]</sup> long fibers or sheets yarned from CNT forests,<sup>[2,3]</sup> solids and wafers densified from aligned films,<sup>[4,5]</sup> solution-processed aerogels<sup>[6]</sup> and thin films or buckypapers,<sup>[7,8]</sup> in which the alignment, density, and porosity of the CNTs can be tailored. These structures demonstrated potential applications in a variety of areas such as supercapacitors,<sup>[4,7]</sup> catalytic electrodes,<sup>[9]</sup> flexible heaters,<sup>[4]</sup> superhydrophobic coatings,<sup>[10]</sup> biomimetic surfaces,<sup>[11]</sup> artificial muscles,<sup>[12]</sup> and integrated microelectromechanical systems.<sup>[5]</sup> The engineered nanostructures offer a great opportunity to develop high-performance materials and explore applications in various fields.

Most importantly, the light-weight, high porosity, and large surface area of CNT-based materials make them a promising candidate for environmental applications such as sorption, filtration and separation.<sup>[13–15]</sup> For example, CNTs were considered as superior sorbents for a wide range of organic chemicals and inorganic contaminants than conventional systems such as clay and activated carbon, with a number of advantages including stronger chemical-nanotube interactions, rapid equilibrium rates, high sorbent capacity and tailored surface chemistry.<sup>[14,15]</sup> Filters based on aligned CNT arrays were used to remove hydrocarbons or bacterial, and separate different-size proteins.<sup>[16,17]</sup> Membranes made from parallel CNT channels with tunable pore size and density have shown high flux for gas and water, and selective molecular transport through pore functionalization.<sup>[18–20]</sup> Despite the attractive physical properties of CNTs and intensive efforts in this area, the progresses in environmental applications have been limited in the sorption or separation of diluted molecules and ions in very small amount or scale.<sup>[21–23]</sup>

Here, we report the synthesis of a sponge-like bulk material consisting of self-assembled, interconnected CNT skeletons, with a density close to the lightest aerogels, a porosity of >99%, high structural flexibility and robustness, and wettability to organics in pristine form. The CNT sponges can be deformed into any shapes elastically and compressed to large-strains repeatedly in air or liquids without collapse. The sponges in densified state swell instantaneously upon contact with organic solvents. They absorb a wide range of solvents and oils with excellent selectivity, recyclability, and absorption capacities up to 180 times their own weight, two orders of magnitude higher than activated carbon. A small densified pellet floating on water surface can quickly remove a spreading oil film with an area up to 800 times that of the sponge, suggesting potential environmental applications such as water remediation and large-area spill cleanup. In comparison, the application of one of the lightest porous materials, silica aerogel, has been impeded by their structural fragility, environmental sensitivity and high production cost.<sup>[24,25]</sup>

Figure 1a shows a macroscopic, monolithic sponge synthesized by chemical vapor deposition (CVD) in which a precursor solution of ferrocene in dichlorobenzene was injected at 860 °C for four hours (see Experimental). Scanning electron microscopy (SEM) characterization shows that the sponge consists of CNTs self-assembled into a porous, interconnected, three-dimensional framework (Fig. 1b). No apparent difference in their morphology and distribution was observed from the top surface or side-walls (Fig. S1). These are multi-walled nanotubes with diameters in the range of 30 to 50 nm (Fig. 1c) and lengths of tens to hundreds of micrometers, indicating there are multiple layers of CNTs existing in the cm-thick sponge. Many catalyst particles were encapsulated inside the tube cavities. The growth rate along the thickness direction is about 2–3 mm per hour, and did not slow down during the entire process therefore the sponge production is scalable (Fig. S1). On the microscale, each CNT makes a high aspect-ratio continuous skeleton, compared with crosslinked nanoparticles in silica aerogels that are inherently brittle. The CVD method is similar to that was reported for growing vertical CNT arrays,<sup>[26]</sup> but we used a different carbon source (dichlorobenzene) to disturb the aligned growth and obtain a randomly interconnected structure. The growth process of the sponges can be seen as a consecutive stacking and penetration of numerous CNT “piles” into centimeter thickness (as illustrated in Fig. 1d), which is substantially different from aligned arrays where most of CNTs grow continuously from the bottom to top surface<sup>[26]</sup> or thin sheets where CNTs were densified into a two-dimensional network during vacuum filtration.<sup>[7,8]</sup>

The bulk density of as-grown sponges is about 5–10 mg cm<sup>-3</sup>, comparable to un-densified vertically aligned arrays (10 mg cm<sup>-3</sup>)<sup>[18]</sup>

[\*] Prof. D. Wu, X. Gui, Prof. J. Wei, Prof. K. Wang, Prof. H. Zhu, Y. Jia, Q. Shu  
Key Laboratory for Advanced Materials  
Processing Technology, Ministry of Education  
Department of Mechanical Engineering, Tsinghua University  
Beijing 100084 (P. R. China)  
E-mail: wdh-dme@tsinghua.edu.cn

Prof. A. Cao  
Department of Advanced Materials and Nanotechnology  
College of Engineering, Peking University  
Beijing 100871 (P. R. China)  
E-mail: anyuan@pku.edu.cn

DOI: 10.1002/adma.200902986

and solution-processed aerogels ( $7.5 \text{ mg cm}^{-3}$ )<sup>[6]</sup> slightly larger than the aerogel sheets drawn from CNT forests ( $1.5 \text{ mg cm}^{-3}$ )<sup>[3]</sup> and the lightest silica aerogels ( $2\text{--}3 \text{ mg cm}^{-3}$ ). They have a surface area of  $300$  to  $400 \text{ m}^2 \text{ g}^{-1}$  and an average pore size of about  $80 \text{ nm}$ , corresponding to the average inter-tube distance observed in SEM. The sponge porosity is estimated to be  $>99\%$  based on calculations using a density of  $1.0\text{--}1.2 \text{ g cm}^{-3}$  for large-cavity CNTs with outer diameters of  $30$  to  $50 \text{ nm}$  and inner diameters of  $20$  to  $35 \text{ nm}$ . SEM examination on cross-sections of a epoxy-filled sponge shows that CNTs occupy less than  $0.5\%$  of the total cross-sectional area in any direction, indicating a very large pore volume. The pristine sponges are hydrophobic with a contact angle of about  $156^\circ$  for water droplets, and can be floated on water surface since their density is only  $1\%$  of the water density. In comparison, a conventional cleaning sponge made from micro polyurethane fibers is hydrophilic and sank below the surface level when in contact with water (Fig. 1e).

The CNT sponges display structural flexibility that was rarely observed in other high-porosity materials (e.g., aerogels) or aligned CNT arrays. Manual compression to  $>50\%$  volume reduction shows that the sponge is compliant and springy (see Supporting Information Movie). A bulk sponge can be bent to a large degree or twisted without breaking apart, and after that still recover to nearly original shape (Fig. 1f and g). Prolonged ultrasonication in solvents did not dismantle the sponges. The structural integrity under large deformations is owing to the highly interconnected CNTs in a three-dimensionally isotropic configuration, which could prevent the sliding or splitting between CNTs along any direction. In contrast, CNT aerogels prepared by solution processing and critical-point-drying are very brittle and need reinforcement by polymer infiltration.<sup>[6]</sup>

By introducing solvents (e.g., ethanol) and then gently compressing the sponge to remove the solvent, we formed densified pellets in dry state with controlled shapes such as flat carpets or spherical particles (Fig. 1h). There is about  $10$  to  $20$  times volume shrinkage during densification and much higher volume reduction is possible by processing in vacuum to make CNTs more densely packed. The densified pellets instantaneously swell to larger sizes by adding droplets of ethanol until recover to the original volume (Fig. 1h), and can be densified again by squeezing out the absorbed solvent for many times, therefore the swelling process is fully reversible. Shape and structural recovery of the sponges stems from the random distribution of CNTs that prevents the formation of strong van der Waals interactions even at densified state, therefore liquid re-absorption into the pores could push CNTs away and back to their original configuration. For other structures such as aligned forests, introduction of liquids zip them into a densely packed solid due to maximum van der Waals

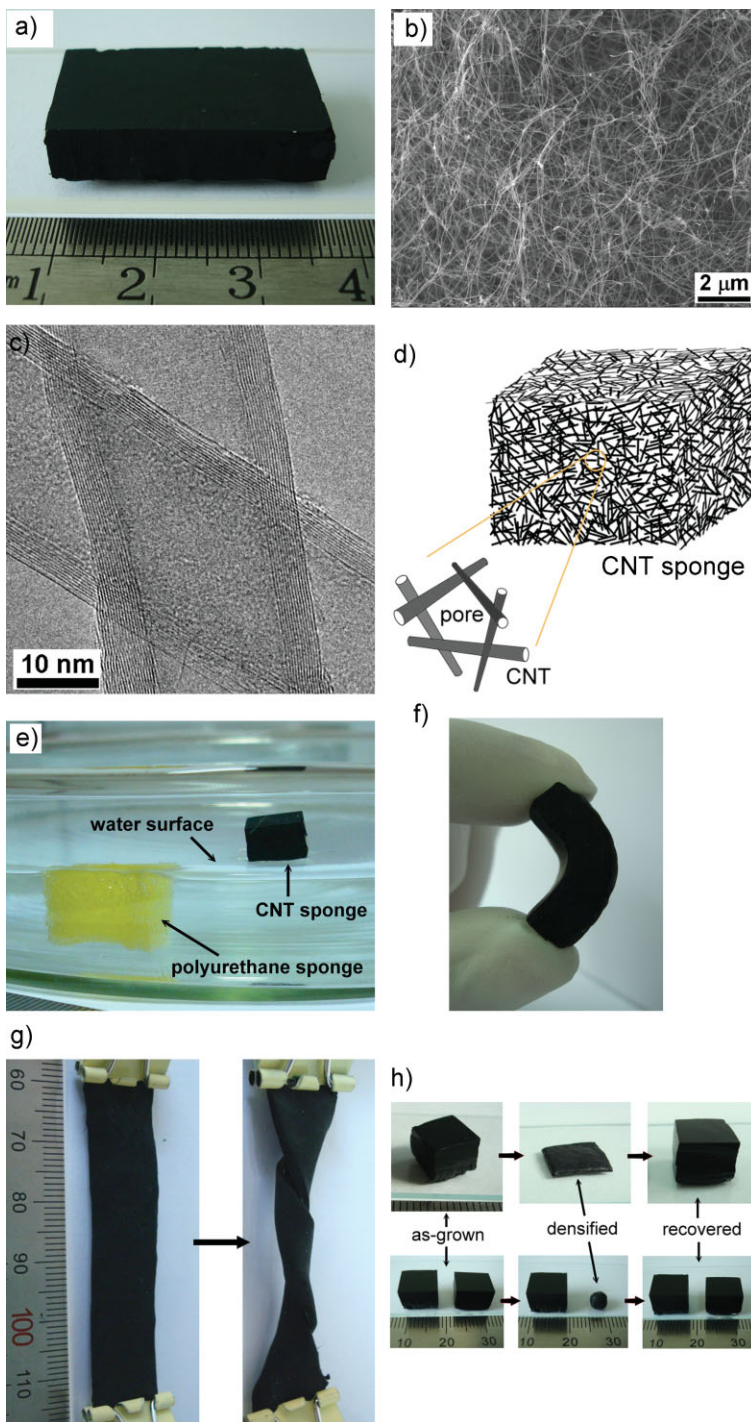


**Figure 1.** Light, porous, flexible carbon nanotube sponges. a) A monolithic sponge with a size of  $4 \text{ cm} \times 3 \text{ cm} \times 0.8 \text{ cm}$  and a bulk density of  $7.5 \text{ mg cm}^{-3}$ . b) Cross-sectional SEM image of the sponge showing a porous morphology and overlapped CNTs. c) TEM image of large-cavity, thin-walled CNTs. d) Illustration of the sponge consisting of CNT piles (black lines) as the skeleton and open pores (void space). e) Picture of a CNT and a polymeric sponge placed in a water bath. The CNT sponge is floating on the top while the polyurethane sponge absorbed water and sank below the surface level. f) A CNT sponge bent to arch-shape at a large-angle by finger tips. g) A  $5.5 \text{ cm} \times 1 \text{ cm} \times 0.18 \text{ cm}$  sponge twisted by three round turns at the ends without breaking. h) Densification of two cubic-shaped sponges into small pellets (a flat carpet and a spherical particle, respectively) and full recovery to original structure upon ethanol absorption.

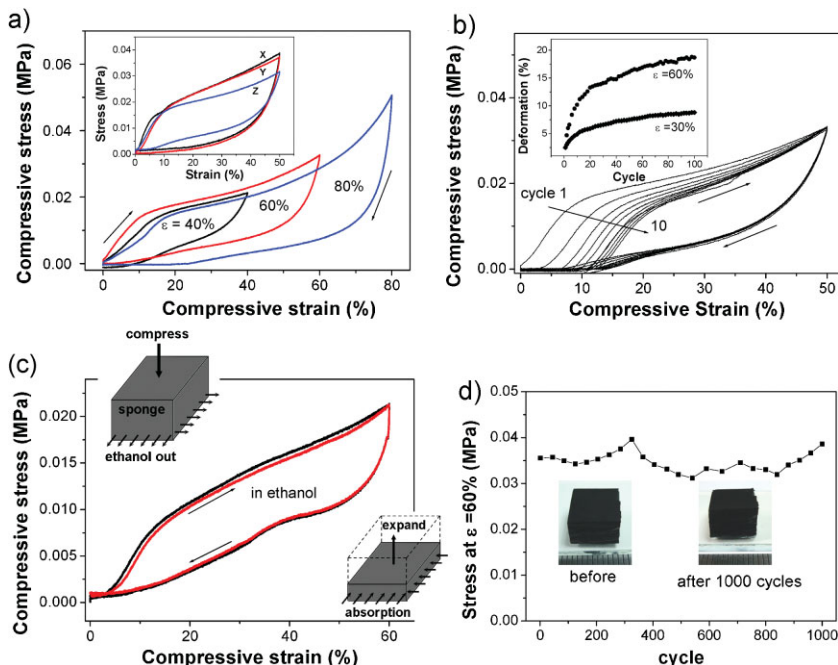


**Figure 2.** Mechanical properties of CNT sponges in air and liquids. a) Loading and unloading compressive stress-strain curves of several sponges at different set strains ( $\varepsilon$ ) of 40%, 60%, and 80%, respectively, showing consistent behavior in which an initial linear region ( $0 < \varepsilon < 18\%$ ) followed by a plateau can be distinguished. The lower stress level ( $< 0.05$  MPa) at maximum strains (up to 80%) indicates the softness and structural flexibility of the sponges. Inset, stress-strain curves recorded by compressing a cubic sponge along three orthogonal directions (X: length, Y: width, Z: thickness) showing a nearly isotropic response. b) Cyclic stress-strain curves at a maximum  $\varepsilon = 50\%$  in air. Inset, recorded deformations developed by compressions for 100 cycles at different set strains of  $\varepsilon = 30\%$  and  $60\%$ , respectively. c) Compression of sponges immersed in ethanol in which loading and unloading curves of two cycles (black and red curves) show full thickness (volume) recovery by ethanol absorption. Insets illustrate the processes of compression (ethanol desorption) and unloading (ethanol absorption). Horizontal arrows indicate the flowing direction of ethanol. The ethanol absorption is accompanied by the fast expansion (vertical arrow) of the compressed sponge into the original volume (dashed box). d) Stress recorded for 1000 cycles at set  $\varepsilon = 60\%$  showing no strength degradation. Inset, photos of the CNT sponge before and after cyclic tests.

forces produced between parallel CNTs, which is a irreversible process.<sup>[4]</sup>

The sponges can sustain large-strain deformations, recover most of the material volume elastically, and resist structural fatigue under cyclic stress conditions, in both air and liquids. Uniaxial compression tests of several samples at differently set strains (40% to 80%) show reproducible results in which all curves contain an initial linear region at  $\varepsilon < 20\%$  and a plateau with gradually increasing slope until very high strains up to 80% (Fig. 2a). For moderate-strain compressions ( $\varepsilon = 40\%$  and  $60\%$ ), the unloading curves are above the axis while returning to the origin, indicating complete volume recovery without plastic deformations. SEM characterization did not reveal much difference of the CNT morphology in fully recovered sponges. The large-degree compression on these sponges is due to the squeezing of inter-tube pores, rather than the formation of heavy buckles along CNTs as observed in aligned films.<sup>[27]</sup> The sponges can be compressed to more than 95% volume reduction ( $\varepsilon > 95\%$ ) at low stress values ( $< 0.25$  MPa), due to their high porosity and structural flexibility. The hysteresis loops in all the samples

indicate substantial energy dissipation due to friction between flowing air and the sponge skeleton, which is a useful property for constructing light-weight, energy absorption layers. In addition, compression along different directions at the same strain ( $\varepsilon = 50\%$ ) reveals an isotropic response in the stress-strain curves, in which the maximum stress (0.03 MPa) along the thickness (direction Z) is very close to that of the other two orthogonal directions (0.037 and 0.038 MPa, respectively) (inset of Fig. 2a). This confirms the spatial uniformity and three-dimensionally isotropic structure of the sponges.

Repeated large-strain compressions in air produced plastic deformation in sponges with a visible thickness reduction, as also seen from the gradual shift of the loading and unloading curves in increasing cycles (Fig. 2b). The sponges can spring back to recover most of thickness and maintain a similar compressive stress (0.032 MPa) at the maximum strain ( $\varepsilon = 50\%$ ) in every cycle, indicating little degradation of mechanical strength. Plastic deformation is measured to be smaller than 8% (of volume reduction) after compressions at a set strain of  $\varepsilon = 30\%$  for 100 cycles, and less than 20% at an increased maximum strain ( $\varepsilon = 60\%$ ) (inset of Fig. 2b). Thickness and volume recovery of the sponges is not due to the straightening of buckled CNTs,<sup>[27]</sup> but rather a coordinated movement of CNT skeletons back to initial configuration which at the same time allows air to fill into the open pores.

We have done similar tests by immersing the samples completely in a solvent (e.g., ethanol) bath, in which ethanol was driven out of the sponge pores during compression, and re-absorbed during unloading and the sponge expansion (Fig. 2c). The stress needed to remove liquid from the sponges ( $\approx 0.02$  MPa) is comparable to that was measured to remove air (0.03 MPa, shown in Fig. 2b), indicating that liquid flow through the interconnected pores is smooth. The sponges readily expand back to original volume by solvent uptake during the unloading process. There was no visible gap between the compression stage and the top surface of the sponge when the stage was set to retreat (unload) at high rates up to  $80 \text{ mm min}^{-1}$  (or  $1.2 \text{ mm s}^{-1}$ ), indicating that the volume expansion is very fast with a thickness-increasing rate of  $> 1.2 \text{ mm s}^{-1}$  by solvent absorption. When compressed in a water bath, the sponges can not expand during unloading due to their hydrophobicity which prevents water absorption. The selective uptake of solvent (in preference to water) is important for environmental applications. The sponges show no strength degradation after compression at a set strain of 60% for 1000 cycles (Fig. 2d), suggesting structural robustness compared with brittle silica aerogels. Interestingly, we did not observe volume reduction of the sponges after they were compressed in solvent for 1000 times (inset of Fig. 2d), while

a deformation of nearly 20% was measured during compression in air as shown in inset of Figure 2b. It shows that the absorption and filling of solvents into the pores is favorable for the sponges to recover the original structure. Reversible absorption and removal of solvents for many times also provides a simple way for recycled use.

The CNT sponges demonstrate high absorption capacities (defined by  $Q$ , the ratio between the final and initial weight after full absorption) of 80 to 180 times their own weight for a wide range of solvents and oils, with larger  $Q$  for higher-density liquids (e.g., chloroform) (Fig. 3a). The mechanism is mainly physical absorption of organic molecules which can be stored in the sponge pores. Owing to the low sponge density and high porosity, the  $Q$  values are significantly higher than the weight gains of dense manganese oxide nanowire membranes (<20 times) made by filtration for similar solvents and oils.<sup>[28]</sup> The absorbed oil or solvents can be removed by mechanical compression or directly burned in air without destroying the sponge structure (Fig. S2). We tested many porous materials with different pore sizes and densities including natural fibrous products (e.g., cotton towel, loofah), polymeric sponges (e.g., polyurethane- or polyester-based) and pellets of activated carbon with a density of  $2000 \text{ mg cm}^{-3}$  (Fig. S3). In case of diesel oil, the absorption capacity of CNT sponges ( $Q = 143$ ) is several times that of polymeric sponges ( $Q < 40$ ), 35 times that of cotton and loofah ( $Q < 4$ ) and two orders of magnitude higher than activated carbon ( $Q < 1$ ) (Fig. 3b).

The CNT sponges in pristine or densified form can actively absorb and remove different type of oils spreading on water surface. Distributing 2.5 mL vegetable oil (density =  $0.9 \text{ g cm}^{-3}$ ) on a water bath makes a thick, disk-shape,  $28 \text{ cm}^2$  film with a thickness in the center part of 2 to 4 mm. A densified sponge in spherical shape (diameter = 8 mm) was placed in the film and suspended on the top. We observed that the oil film kept shrinking toward the center while the sponge grew to a larger size due to oil absorption (Fig. 3c). After uptake of the entire oil film, the sponge still floating on water has recovered to nearly original shape and size ( $3 \text{ cm} \times 2 \text{ cm} \times 0.6 \text{ cm}$ ). In addition, a piece of pristine sponge can continuously attract and suck most part of an oil film when it was placed to contact the edge of the film (Fig. 3d). Significantly, a small particle of densified CNT sponge (with a diameter of 6 mm and a volume of  $\sim 0.1 \text{ cm}^3$ ) can remove a spreading diesel oil film with an area of  $227 \text{ cm}^2$  in several minutes (Fig. 3e). We observed that the sponge was floating on water surface and moving freely throughout the

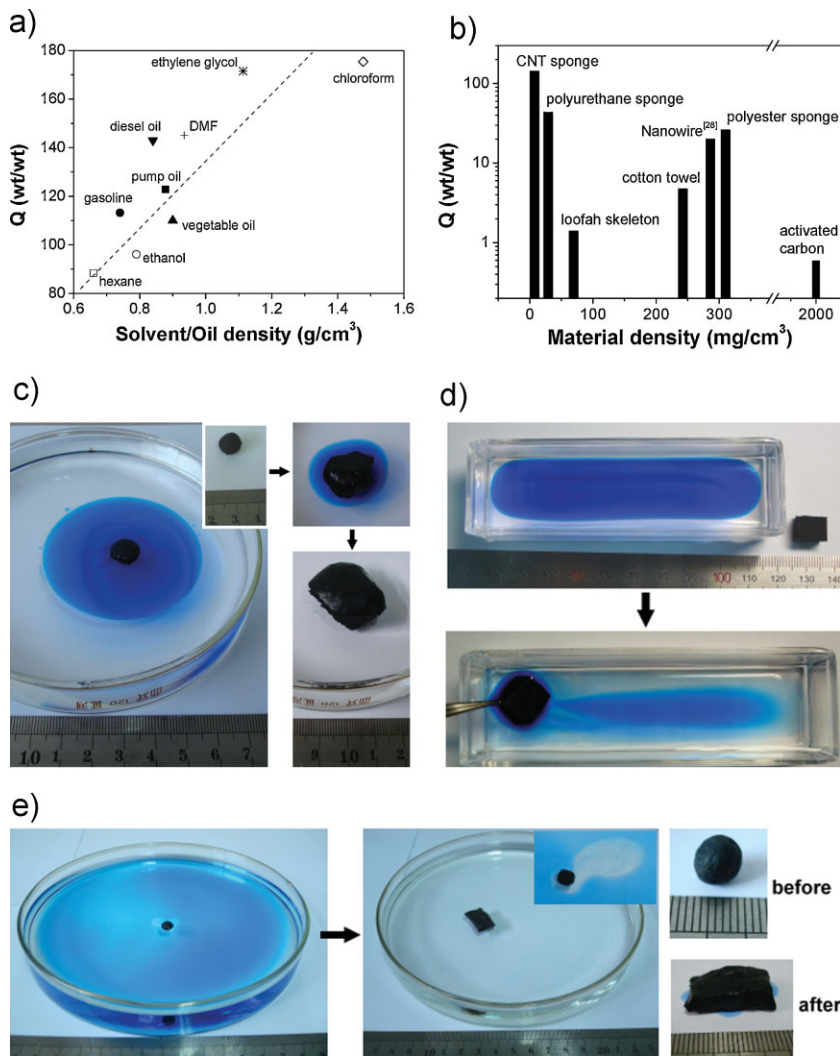


**Figure 3.** Environmental application of CNT sponges. a) Absorption capacity ( $Q$ ) measured for a range of oils (solid symbols) and organic solvents. The dashed line indicates increasing absorption capacity for higher-density liquids. b) Summary of the absorption capacity for diesel oil measured from CNT sponges, natural products (cotton, loofah), polymeric sponges (polyurethane, polyester) and activated carbon. The maximum weight gain for oils by previously reported nanowire membranes ( $Q = 20$ ) (ref. [27]) is included for comparison. c) Snapshots showing the absorption of a  $28 \text{ cm}^2$  and mm-thick vegetable oil film (dyed with Oil Blue) distributed on a water bath by a small spherical sponge. The growing size of the sponge accompanied by the shrinkage of oil film indicates continuous oil absorption and storage inside the water channel. d) Active absorption of a continuous  $20 \text{ cm}^2$  oil strip distributed in a rectangular water channel by a small non-densified sponge ( $< 1 \text{ cm}^3$ ) placed near the left edge and in contact with oil. e) Large-area oil cleanup. (left panel) A diesel oil film ( $2 \text{ g}$  in total weight) with an area of  $227 \text{ cm}^2$  spreading on water and a densified sponge pellet placed in the center. The oil area is about 800 times that of the projected sponge area. (middle) Clean water surface after complete oil absorption by the sponge, which has grown to a larger size and changed to a rectangular shape. Inset shows the floating pellet during the absorption process. The white-color region along the path of the drifting pellet indicates the removal of oil film and exposure of fresh water. (right) Pictures of the CNT sponge before and after absorption. The sponge has swollen from a 6-mm-diameter spherical particle to a rectangular monolith ( $2 \text{ cm} \times 1.4 \text{ cm} \times 0.6 \text{ cm}$ ) after collecting all the oil from water.

oil area. Wherever it arrived, the sponge instantaneously sucked the part of oil film in contact, resulting in a local white-color region around and behind where fresh water exposed. The sponge tends to drift to the remaining oil film area due to its

water-repelling and oil-wetting properties, leading to this unique “floating-and-cleaning” capability that is particularly useful for spill cleanup. The sponge expanded into a volume of  $2\text{ cm} \times 1.4\text{ cm} \times 0.6\text{ cm}$  after absorption of the whole oil film (about 2 g), leaving a clear water surface around. The oil area that has been completely cleaned is about 800 times larger than the size of the initial densified sponge.

The CNT sponge is a good low-density thermal insulator, with measured thermal conductivity of less than  $0.15\text{ W} \cdot \text{K}^{-1} \text{ m}^{-1}$  at temperatures of 200 K to 360 K (Fig. S4), comparable to other insulate materials such as woods, ceramic and polymeric foams ( $0.02\text{--}1\text{ W} \cdot \text{K}^{-1} \text{ m}^{-1}$ ). Although individual CNTs are good thermal conductors, the ultrahigh porosity of the sponge make it a good thermal insulator. The electrical resistivity is about  $6 \times 10^{-3}\ \Omega\text{ m}$  based on a two-probe measurement. Compared with conventional porous materials, CNT sponges offer additional advantages such as mechanical flexibility and robustness, electrical conductivity, thermal stability and resistance to harsh environment, and can impact a broad range of applications such as multifunctional structural media, sensors, high strength-to-weight ratio composites, membranes and electrodes.

## Experimental

**Synthesis of CNT Sponges:** CNT sponges were synthesized by CVD process using ferrocene and 1,2-dichlorobenzene as the catalyst precursor and carbon source, respectively. Ferrocene powders were dissolved in dichlorobenzene to make a solution at a concentration of  $0.06\text{ g ml}^{-1}$ , which was then continuously injected into a 2-inch quartz tube housed in a resistive furnace by a syringe pump at a feeding rate of  $0.13\text{ ml min}^{-1}$ . The reaction temperature was set as  $860\text{ }^\circ\text{C}$ . Carrier gas, a mixture of Ar and  $\text{H}_2$ , was flowing at a rate of  $2000\text{ ml min}^{-1}$  and  $300\text{ ml min}^{-1}$ , respectively. A 2 inch  $\times$  1 inch quartz sheet was placed in the reaction zone as the growth substrate. The sponge-like products were collected from the quartz substrate after CVD, which typically reach a thickness of 0.8 to 1 cm for a growth period of 4 hours.

**Characterization of CNT Sponges:** The sponge morphology and CNT structure was characterized by SEM (Leo 1505) and TEM (JEOL 2011). Mechanical tests were carried out by Instron 5843 equipped with two flat-surface compression stages and 10 N/1 kN load cells. CNT sponges were cut into cubic (about  $1\text{ cm} \times 1\text{ cm} \times 1\text{ cm}$ ) or rectangular blocks. To compress the sponges in liquid (e.g., ethanol or water), a glass dish with a liquid bath was placed on the bottom stage, and a sponge was placed in the bath. The sponge was completely immersed in the liquid during the compression cycles, and the sponge can only expand its volume from the compressed state by absorbing surrounding liquid during unloading. The top compression stage was modified to the same cross-sectional size to the sponge sample to avoid direct compression on liquid surface and minimize the effects of incompressible liquid on the mechanical tests.

**Solvent and Oil Absorption of CNT Sponges and other Porous Materials:** We measured the absorption capacity of the CNT sponges for various organic solvents and oils with different densities, including ethanol (density =  $0.79\text{ g cm}^{-3}$ ), hexane ( $0.66\text{ g cm}^{-3}$ ), DMF ( $0.94\text{ g cm}^{-3}$ ), ethylene glycol ( $1.11\text{ g cm}^{-3}$ ), chloroform ( $1.48\text{ g cm}^{-3}$ ), gasoline ( $0.74\text{ g cm}^{-3}$ ), pump oil ( $0.88\text{ g cm}^{-3}$ ), diesel oil ( $0.84\text{ g cm}^{-3}$ ) and vegetable oil ( $0.90\text{ g cm}^{-3}$ ). Pristine CNT sponges cut in cubic shape were placed inside the solvents and oils for a set time (e.g., 15 seconds) and then picked out for measurements. The absorption is very fast and typically reaches saturation within a few seconds by immersing the sponge into the liquid. The sponge weights after and before absorption were recorded for calculating Q values. Weight measurements were done quickly to avoid evaporation of absorbed solvents or oils. Other porous materials such as

polymeric sponges, loofah, and activated carbon were tested with the same procedure as used for the CNT sponges.

## Acknowledgements

We thank L. Fan and L. Liu for the discussion of experiments. J. Wei thanks NSFC (grant no: 50672047) for funding support. A. Cao thanks the College of Engineering in Peking University for starting-up support. Supporting Information is available online from Wiley InterScience or from the author.

Received: August 30, 2009

Published online: November 9, 2009

- [1] K. Hata, D. N. Futaba, K. Mizuno, T. Namai, M. Yumura, S. Iijima, *Science* **2004**, *306*, 1362.
- [2] M. Zhang, K. R. Atkinson, R. H. Baughman, *Science* **2004**, *306*, 1358.
- [3] M. Zhang, S. Fang, A. A. Zakhidov, S. B. Lee, A. E. Aliev, C. D. Williams, K. R. Atkinson, R. H. Baughman, *Science* **2005**, *309*, 1215.
- [4] D. N. Futaba, K. Hata, T. Yamada, T. Hiraoka, Y. Hayamizu, Y. Kakudate, O. Tanaike, H. Hatori, M. Yumura, S. Iijima, *Nat. Mater.* **2006**, *5*, 987.
- [5] Y. Hayamizu, T. Yamada, K. Mizuno, R. C. Davis, D. N. Futaba, M. Yumura, K. Hata, *Nat. Nanotechnol.* **2008**, *3*, 289.
- [6] M. B. Bryning, D. E. Milkie, M. F. Islam, L. A. Hough, J. M. Kikkawa, A. G. Yodh, *Adv. Mater.* **2007**, *19*, 661.
- [7] R. N. Das, B. Liu, J. R. Reynolds, A. G. Rinzler, *Nano Lett.* **2009**, *9*, 677.
- [8] M. Endo, H. Muramatsu, T. Hayashi, Y. A. Kim, M. Terrones, M. S. Dresselhaus, *Nature* **2005**, *433*, 476.
- [9] J. E. Trancik, S. C. Barton, J. Hone, *Nano Lett.* **2008**, *8*, 982.
- [10] K. K. S. Lau, J. Bico, K. B. K. Teo, M. Chhowalla, G. A. J. Amaratunga, W. I. Milne, G. H. Mckinley, K. K. Gleason, *Nano Lett.* **2003**, *3*, 1701.
- [11] L. Qu, L. Dai, M. Stone, Z. Xia, Z. L. Wang, *Science* **2008**, *322*, 238.
- [12] A. E. Aliev, J. Oh, M. E. Kozlov, A. A. Kuznetsov, S. Fang, A. F. Fonseca, R. O valle, M. D. Lima, M. H. Haque, Y. N. Gartstein, M. Zhang, A. A. Zakhidov, R. H. Baughman, *Science* **2009**, *323*, 1575.
- [13] M. A. Shannon, P. W. Bohn, M. Elimelech, J. G. Georgiadis, B. J. Mariñas, A. M. Mayes, *Nature* **2008**, *452*, 301.
- [14] M. S. Mauter, M. Elimelech, *Environ. Sci. Technol.* **2008**, *42*, 5843.
- [15] B. Pan, B. Xing, *Environ. Sci. Technol.* **2008**, *42*, 9005.
- [16] A. Srivastava, O. N. Srivastava, S. Talapatra, R. Vajtai, P. M. Ajayan, *Nat. Mater.* **2004**, *3*, 610.
- [17] X. Li, G. Zhu, J. S. Dordick, P. M. Ajayan, *Small* **2007**, *3*, 595.
- [18] M. Yu, H. H. Funke, J. L. Falconer, R. D. Noble, *Nano Lett.* **2009**, *9*, 225.
- [19] J. K. Holt, H. G. Park, Y. Wang, M. Stadermann, A. B. Artyukhin, C. P. Grigoropoulos, A. Noy, O. Bakajin, *Science* **2006**, *312*, 1034.
- [20] B. J. Hinds, N. Chopra, T. Rantell, R. Andrews, V. Gavalas, L. G. Bachas, *Science* **2004**, *303*, 62.
- [21] W. Chen, L. Duan, D. Zhu, *Environ. Sci. Technol.* **2007**, *41*, 8295.
- [22] X. Peng, Y. Li, Z. Luan, Z. Di, H. Wang, B. Tian, Z. Jia, *Chem. Phys. Lett.* **2003**, *376*, 154.
- [23] R. Q. Long, R. T. Yang, *J. Am. Chem. Soc.* **2001**, *123*, 2058.
- [24] N. Leventis, C. Sotiriou-Leventis, G. Zhang, A.-M. M. Rawashdeh, *Nano Lett.* **2002**, *2*, 957.
- [25] L. A. Capadonna, M. A. B. Meador, a. Alunni, E. F. Fabrizio, P. Vassilaras, N. Leventis, *Polymer* **2006**, *47*, 5754.
- [26] R. Andrews, D. Jacques, A. M. Rao, F. Derbyshire, D. Qian, X. Fan, E. C. Dickey, J. Chen, *Chem. Phys. Lett.* **1999**, *303*, 467.
- [27] A. Cao, P. L. Dickrell, W. G. Sawyer, M. N. Ghasemi-Nejhad, P. M. Ajayan, *Science* **2005**, *310*, 1307.
- [28] J. Yuan, X. Liu, O. Akbulut, J. Hu, S. L. Suib, J. Kong, F. Stellacci, *Nat. Nanotechnol.* **2008**, *3*, 332.